

## **Drying Effects on Corrosion Properties of Cr(VI)- and Cr(III)-Treated Electrogalvanized Steel**

Xiaolong Zhang, Chris van den Bos, Wim G. Sloof, Arjan Hovestad, Herman Terryn and J.H.W. De Wit

*ECS Trans.* 2006, Volume 1, Issue 9, Pages 165-176.  
doi: 10.1149/1.2215586

---

**Email alerting  
service**

Receive free email alerts when new articles cite this article - sign up in the box at the top right corner of the article or [click here](#)

---

---

To subscribe to *ECS Transactions* go to:  
<http://ecst.ecsdl.org/subscriptions>

---

## **DRYING EFFECTS ON CORROSION PROPERTIES OF CR(VI)- AND CR(III)-TREATED ELECTROGALVANIZED STEEL**

X. Zhang<sup>(1,2)</sup>, C. van den Bos<sup>(2)</sup>, W.G. Sloof<sup>(2)</sup>, A. Hovestad<sup>(3)</sup>, H. Terryn<sup>(1)</sup> and J.H.W. de Wit<sup>(1, 2)</sup>

<sup>(1)</sup> Netherlands Institute for Metals Research (NIMR), Mekelweg 2, P.O. Box 5008, 2600 GA Delft, The Netherlands

<sup>(2)</sup> Department of Materials Science, Delft University of Technology, Mekelweg 2, 2628 CD Delft, The Netherlands

<sup>(3)</sup> TNO Science and Industry, P.O. Box 6235, 5600 HE Eindhoven, The Netherlands

### **ABSTRACT**

Drying effects on corrosion performance of Cr(VI)- and Cr(III)-treated electro-galvanized steel have been studied in NaCl solution using potentiodynamic measurements and electrochemical impedance spectroscopy (EIS). The Cr(VI) and the Cr(III) treated specimens were dried at three different temperatures: 60, 110 and 210°C. The surface layers were investigated using SEM, AES and XPS. The results show that the drying temperature not only affects the morphology of the surface layer, but also changes the chromium oxidation states in the layer. The corrosion protection given to the EG steel by Cr(VI) and Cr(III) pretreatments can be severely reduced if the pretreated surfaces are heated above 110°C. Both types of coating undergo some dehydration during heat treatments, which is undesirable for good corrosion protection. For Cr(VI) coatings, additional degradation mechanisms include widening of the cracks in the coating, and reduction of Cr(VI) to the Cr(III) oxidation state.

### **INTRODUCTION**

Zinc coating is widely used to protect carbon steel against corrosion. The zinc coatings on electrogalvanized steel (EGS) are usually not as thick as those on hot dip galvanized steel and are mainly used as a base for paint (1). In order to increase the corrosion resistance and improve the adhesion to paints, zinc coatings need more pretreatments such as phosphate and chromate conversion coatings. Chromate conversion coating is widely used in metal finishing industry. However, the toxicity of hexavalent chromium involved in this treatment necessitates a search for replacements (2, 3). As one of potential alternatives to conventional Cr(VI) treatments, trivalent chromium treatment is regarded as commercially acceptable for certain applications in zinc finishing industry (4).

The thermal stability of conversion coatings is interesting because passivated metal parts have to endure heat treatment during the fabrication of assemblies. Previous work showed that drying of the chromate coatings may affect the corrosion performance of the coatings (5-7).

Laget et al. (5) observed that heating and aging the chromate coating on Al-2024 alloys degraded the coatings, while Gallaccio et al. (7) found that heating and aging the chromate coatings on magnesium increased their corrosion resistance. In this paper, we report on studies of the surface structure and electrochemical behavior of Cr(VI) and Cr(III) treated electro-galvanized steel (EGS) changing with the heating temperature, aimed at understanding the influence of the thermal effect on the corrosion performance of the Cr(VI) and the Cr(III) coatings in a solution containing chloride.

## EXPERIMENTAL

**Materials.** Electro-galvanized steel ( $\sim 13 \mu\text{m}$  thick zinc coating) was activated in 0.25%  $\text{HNO}_3$  solution for 30 seconds and rinsed in de-ionized water. For the purpose of doing surface analysis, pure zinc sheets (0.5 mm thick) were polished to  $1 \mu\text{m}$  and ultrasonically cleaned in acetone and alcohol for 2 minutes, respectively. Cr(VI) treatment was carried out on the EGS and pure zinc sheets in a bath containing 200 g/L  $\text{Na}_2\text{Cr}_2\text{O}_7 + 10 \text{ g/L } \text{H}_2\text{SO}_4$  (pH 1.2) for different dipping times. The Cr(VI)-treated samples were rinsed in de-ionized water and heated in an oven at 60, 110 and  $210^\circ\text{C}$  for 30 minutes. The Cr(III) treatment was carried out in a commercial bath (Permapass 3K, pH 1.8), which contains fluoride and sulfate as accelerators. After rinsing in de-ionized water and drying in flowing air, the Cr(III) treated specimens were heated in an oven either at 70, 110 or  $210^\circ\text{C}$  for 30 minutes.

**Surface Analyses.** The morphology and compositions of the Cr(VI) and the Cr(III) treated samples were analyzed using SEM, AES and XPS. The SEM analysis was performed on a scanning electron microscope, JSM-6500F.

For AES analysis, a 40 nm gold layer was deposited on the Cr(VI) and Cr(III) treated zinc in order to increase the conductivity of the surface. The AES analysis was performed using a PHI 4300 SAM with a  $\text{LaB}_6$  cathode. A cylindrical mirror analyser (CMA) and a 5 keV ion-gun (PHI 04-303) were used. The capture angle of the CMA was  $42^\circ \pm 6^\circ$ . The spectrometer (CMA) was calibrated according to the method described in reference (8). The base pressure in the analysis chamber was  $3 \times 10^{-10}$  Torr. A primary electron beam with energy of 5 keV and a current of  $1 \mu\text{A}$  was incident on the sample surface at  $30^\circ$  to the normal. All the Auger electron spectra were acquired with an energy analyser resolution of  $\Delta E/E = 0.6\%$ .

Alternate sputtering and data acquisition were performed to obtain the depth profile for two locations on each sample. The surface was rastered using a 2 keV Ar ion beam over an area of  $4 \times 4 \text{ mm}^2$ . The emission current was 20 mA and Ar pressure was 10 mPa. The ion beam was used at intervals of 1 minute and impinged on the sample surface at  $50^\circ$  to the normal. The Auger electron spectral regions recorded in the depth profiling are reported in previous work (9). Within each of these acquisition regions, data were

recorded at 1.0 eV intervals except in the O1s region where a 0.5 eV interval was used. The recorded spectra were analysed with Multipak 6.1A software (Physical Electronics). Firstly, the spectra were differentiated using a five-point Savitsky-Golay method (10). The energy range for each element was redefined in order to isolate the peak for the transition of different elements. For Zn, a linear least square fitting was performed to separate zinc metal from zinc oxide (10).

XPS analysis was carried out with a PHI 5400 ESCA using 400 Watt Mg  $K_{\alpha}$  X-rays (1253.6 eV). This instrument is equipped with a Spherical Capacitor Analyzer (SCA) operating with a constant pass energy value. The energy scale of the spectrometer was calibrated according to the method described by Anthony *et al.* (11). Overview spectra were obtained in the range of 0 – 1100 eV with an analyzer pass energy of 71.55 eV. The intensities of Cr 2p, O 1s, C 1s, S 2p and Zn 2p photoelectron lines were recorded separately with an analyzer pass energy of 35.75 eV. The electrons emitted from the specimens were detected at an angle of 45° with respect to the specimen surface. The C 1s peak (284.8 eV) was used as a reference to correct for electrostatic charging. The X-ray satellites, present in all measured spectra as a consequence of the non-monochromatic nature of the incident X-ray beam, were removed using the relative height and displacements with respect to the height and position of the Mg  $K_{\alpha}$ . In order to assess the relative amounts of the species constituting the photoelectron lines, curve fitting was performed with symmetrical Gaussian-Lorentzian peaks after smoothing of the curve and Shirley-type subtraction of the background. The number of components to be fitted to any particular spectrum was determined by choosing the fit with the minimum reduced chi-squared value ( $\chi^2$ ).

Corrosion Measurements. The corrosion behavior of specimens in NaCl solutions was investigated using d.c. polarization and a.c. impedance measurements. Open-circuit potential (OCP) and potentiodynamic polarization measurements were carried out in a cell containing a platinum counter electrode and a reference electrode (saturated calomel electrode:  $E_0 \approx 0.241 \text{ V}_{\text{NHE}}$ ). Cr(VI) treated specimens were immersed in 3.5% NaCl solution (pH 6) for 1 hour to establish a relatively steady open-circuit potential (OCP). Anodic polarization measurements were then obtained by scanning the potential from – 0.25 V versus OCP and ending at 1.0 V versus OCP. Cathodic polarization curves were obtained for the Cr(III) treated EGS in 0.01 M NaCl solution by scanning the potential from OCP and ending at -0.25V versus OCP. The scan rate was 0.167 mV/s.

Electrochemical impedance spectroscopy (EIS) measurements were carried out in 3.5% NaCl solution after immersion for 2 hours at open circuit. The counter electrode was a flat circular platinum net, parallel to the surface of the zinc specimens. The reference electrode was an Ag-AgCl/Cl<sup>-</sup> (saturated KCl) electrode ( $E_0 \approx 0.197 \text{ V}_{\text{NHE}}$ ). The impedance response was analyzed using a Solartron 1255 frequency response analyzer coupled with a Solartron 1287 electrochemical interface in the frequency range of 60 kHz – 0.1 Hz with 5 mV a.c. amplitude versus the OCP.

## RESULTS AND DISCUSSIONS

### Surface Analyses

**Morphology.** Fig. 1 shows the topographic images for the Cr(VI) treated EGS specimens heated at (a) 60, (b) 110 and (c) 210°C. All the Cr(VI)-treated samples dried at different temperatures showed microcracks in the coatings. For the samples dried at 110°C (EGCr110), the size of the microcracks was similar to the cracks in the samples dried at 60°C (EGCr60), but the density of cracks (the length of crack per unit area) was slightly lower. The width of the cracks in the sample dried at 210°C (EGCr210) was larger than that of the EGC60 and the EGC110 samples. EDS analysis showed the presence of C, O, Cr, Zn and S in the surface layer. The carbon and zinc content increased with the raising of the drying temperature, while the oxygen content decreased. The oxidation of Zn would result in an increase of the oxygen content, but due to the dehydration of the chromate layer the net result was a loss of oxygen. In the cracks, the EDS spectrum showed that the chromium and oxygen contents were lower than those in the flat area, while the zinc content was higher. Moreover, zinc oxides (white) were visible along the cracks in the EGC210 samples under the electron microscope.

Fig. 2 shows the topographic images for the Cr(III) treated EGS specimens heated at (a) 70, (b) 110 and (c) 210°C. The conversion layer was so thin that white zinc oxide can be seen in the layer. There were no cracks in the layers. After heating at 210°C for 30 minutes, more white zinc oxide was present on the surface.

**AES analysis.** Fig. 3 shows the AES depth profiles for (a) a Cr(VI) coating and (b) a Cr(III) coating on zinc. For the Cr(VI) coating with dipping time of 10 s, a longer sputtering time is needed than for the Cr(III) coating with dipping time of 60 s. The depth-profiles show that zinc oxide in the top layer of the Cr(VI) coating is less than 4%. The Cr(III) coating contains a mixture of chromium oxides and zinc oxide through the layer, and the content of zinc oxide is more than chromium oxides.

**XPS analysis.** Overview XPS spectra acquired from a Cr(VI) coating showed that there are C, Cr, O and S on the surface. The C is considered to be due to exposure to ambient air. For the Cr(III) coating on zinc, a strong signal from Zn was also detected besides Cr, O and S. It means that zinc oxides/hydroxides also exist within the surface layer of these coatings.

Fig. 4 shows the Cr 2p spectra acquired from the Cr(VI) coating heated at 60°C and the Cr(III) coatings heated at 70°C. For the Cr(VI) coating, the peak at the binding energy of 579.2 eV is attributable to Cr(VI) (12-14). For the Cr(III) coatings, no Cr(VI) peak was observed near 579.2 eV, which means that there is no Cr(VI) in the layer. The Cr 2p<sub>3/2</sub> curves were fitted for chromium in the form of Cr<sub>2</sub>O<sub>3</sub> (576.3 ± 0.2 eV), Cr(OH)<sub>3</sub> or CrOOH (577.4 ± 0.2 eV) and Cr(VI) (579.2 ± 0.2 eV) in the chromate layer (12-15). The fitting results show that the ratio of Cr(VI) to total Cr is about 0.4. About 40% of the Cr is in the form Cr(OH)<sub>3</sub>, and 20 % in Cr<sub>2</sub>O<sub>3</sub>. For the Cr(III) coating on zinc, no Cr(VI) is present in the surface layer. About 60% of the chromium in the Cr(III) coating is in the form of Cr(OH)<sub>3</sub>, and about 40% is in the form of Cr<sub>2</sub>O<sub>3</sub>.

Fig 5 shows the Cr 2p spectra for the Cr(VI) coatings heated at different temperatures. The fitting results show that by increasing the temperature from 60 to 110 and 210°C, the ratio of Cr(VI) to total chromium in the Cr(VI) coating decreased from 35% to 32% and 12%, respectively.

The O 1s spectrum for the chromate coatings was fitted with three components at 530.1, 531.3 and 533.1 eV for oxide anions, hydroxyl groups and adsorbed water, respectively(12). The adsorbed water is about 17%, 15% and 9% in the samples heated at 60, 110°C and 210°C, respectively.

### Corrosion Behavior

For the Cr(VI)-treated EGS specimens heated at different temperatures, the polarization curves measured in 3.5% NaCl solution are shown in Fig. 6. The corrosion current density can be estimated from the slopes of the relevant anodic and cathodic polarization curves within a range of 10 mV from the free corrosion potential using Stern-Geary equation,  $i_{\text{corr}} = k/R_p$ , where  $k$  is a proportionality constant. The constant  $k$  is about 10 mV for zinc in near-neutral NaCl solution (16, 17). The current densities plotted in Fig. 6 and listed in Table 1 are the mean current densities over the specimen surface. All the chromated samples showed lower corrosion currents ( $i_{\text{corr}}$ ) than the untreated EGS samples, and the samples dried at 60°C (EGCr60) showed the lowest  $i_{\text{corr}}$ .

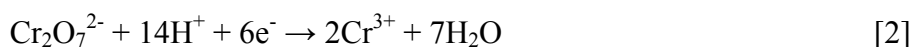
Table 1. Corrosion potential and corrosion current density calculated from the polarization curves in Fig. 6.

Sample	$E_{\text{corr}}$ (V <sub>SCE</sub> )	$i_{\text{corr}}$ ( $\mu\text{A}/\text{cm}^2$ )
EGCr(VI) 60(°C )	-1.04	$0.14 \pm 0.08$
EGCr(VI) 110(°C)	-1.02	$0.3 \pm 0.2$
EGCr(VI) 210(°C)	-1.03	$1.4 \pm 0.6$
EGS	-1.06	$3.0 \pm 0.8$

It is worth noting that for the Cr(VI)-treated samples dried at 60°C (EGCr60), a short passivation process in solution has been observed. For the EGS samples, the current increases with the potential at the beginning of the scan starting at the cathodic branch for a short time. This may be related to the reduction of hexavalent chromium to Cr(III)(18), which adds to the cathodic current. The reduction of Cr(VI) to Cr(III) can contribute to the formation of a passive layer at defects. The cathodic reactions (19), such as



or/and



will consume hydrogen ions and locally increase the pH value, which enables a better passivation process.

Fig. 7 shows the Bode impedance plots for the Cr(VI) treated EGS specimens heated at different temperatures: (a) 60, (b) 110, (c) 210°C and for untreated EGS (d), which were measured after immersion in the quiescent 3.5% NaCl solution (pH 6) for 2 and 4 hours (black lines for 2 hours and dark gray lines or dots for 4 hours). For the Cr(VI)-treated EG steel, the corrosion process occurs on the zinc surface exposed to the electrolyte through pores or defects of the layer. The shape of the Bode plots suggests that there are three time constants for the Cr(VI) treated specimens. The time constant at high frequency side is attributed to the conversion layer, the one at low frequency side is attributed to diffusion phenomenon. The other one is attributed to the double layer. The charge transfer resistance decreased and the diffusion resistance increased within 4 hours. For the Cr(VI) treated EGS specimen heated at 210°C, the capacitance of the conversion layer is larger and the resistances is smaller than for the coatings heated at 60 or 110°C. This suggests that the coatings have become thinner after drying at higher temperatures, and that the cracks in the layer make the real exposure area larger. The wider and deeper cracks observed in the EGCr210 samples by SEM (see Fig. 1) give a piece of evidence of the layer having larger real surface area which can be exposed to the solution. The Cr(VI) treated EGS specimen heated at 60°C showed the largest impedance magnitude. The impedance magnitude shown in Fig. 7 decreases in the following order:  $|Z|(\text{EGCr60}) > |Z|(\text{EGCr110}) > |Z|(\text{EGCr210}) > |Z|(\text{EGS})$ , which is consistent with the polarization results.

For the Cr(III) treated EGS specimens, cathodic polarization curves were measured after immersion in 0.01 M NaCl solution for 1 hour. Fig. 8 shows the cathodic polarization curves for the Cr(III) treated specimens heated at (a) 70, (b) 110, (c) 210°C and for the untreated EGS (d). It shows that the Cr(III) treated specimens heated at 70°C has the lowest cathodic current density. With increase of the drying temperature, the cathodic current density increases. The specimen heated at 210°C had a cathodic reaction rate as large as for the untreated EGS specimen.

Both the polarization and the EIS measurements show that the corrosion rate of the EGS is inhibited by both Cr(VI) and Cr(III) treatments. Increasing the heating temperature results in an increase of the corrosion current for the Cr(VI) and the Cr(III) treated EGS. A Cr(III) coating on the EGS can act as a barrier layer that hinders the transport of oxygen to the underneath metal substrate. Drying the coating at a high temperature (210°C) would degrade the coating, because heating results in more defects in the layer. For the Cr(VI) treated system, the conversion coating contains both Cr(VI) and Cr(III) species. High drying temperature would affect the morphology of the coating and also result in the reduction of the Cr(VI) species adsorbed in the layer, which were confirmed by the SEM and the XPS analyses. The Cr(VI) concentration decrease with the heating temperature has also been observed by Laget et al. (5) on the chromated Al alloys using XANES. During the drying process, the structure of the conversion layer changes due to dehydration. Zinc oxide is a n-type semiconductor and chromium oxides are highly imperfect, so that it is possible for electrons passing through the film to reach Cr(VI) species, which leads to reduction of Cr(VI) to Cr(III). Gallaccio (7) and Xia et al. (20) observed a decrease of release of Cr(VI) in solution for CCCs on zinc and

aluminium after heating. In any case, if there is less soluble Cr(VI) species in the layer, the “self-healing” effect of the coating would diminish.

## CONCLUSIONS

Cr(VI) and Cr(III) treatments can increase the corrosion resistance of EG steel. The corrosion protection given to EG steel by Cr(VI) and Cr(III) pretreatments can be severely reduced if the pretreated surfaces are heated above 110°C. Both types of coating undergo some dehydration during heat treatments, which is undesirable for good corrosion protection. For Cr(VI) coatings, additional degradation mechanisms include widening of the cracks in the coating, and reduction of Cr(VI) to the Cr(III) oxidation state.

## ACKNOWLEDGEMENTS

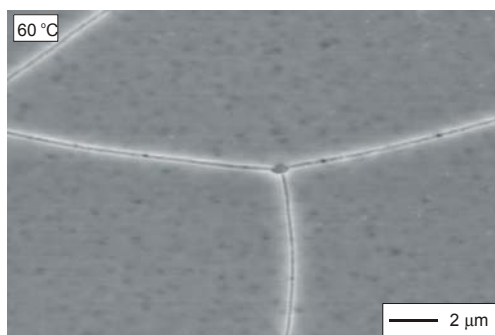
This research was supported by the Dutch Ministry of Economic Affairs (Innovation-directed Research Program for Environmental Technology/Heavy Metals, project IZW98102).

## REFERENCES

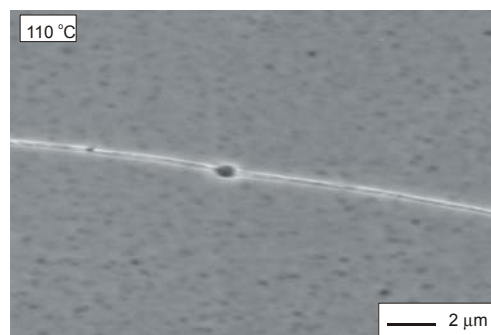
1. D. C. H. Nevison, in *Asm Handbook*, Vol. 9th, p. 755, ASM International, Materials Park, Ohio (1987).
2. R. L. Twite and G. P. Bierwagen, *Prog. Org. Coat.*, **33**, 91 (1998).
3. M. W. Kendig and R. G. Buchheit, *Corrosion*, **59**, 379 (2003).
4. P. C. Wynn and C. V. Bishop, *Trans IMF*, **79**, B27 (2001).
5. V. Laget, C. S. Jeffcoate, H. S. Isaacs, and R. G. Buchheit, *J. Electrochem. Soc.*, **150**, B425 (2003).
6. X. Zhang, S. Bohm, A. J. Bosch, E. R. M. van Westing, and J. H. W. de Wit, *Materials and Corrosion-Werkstoffe Und Korrosion*, **55**, 501 (2004).
7. A. Gallaccio, F. Pearlstein, and M. R. D'Ambrosio, *Metal Finishing*, 50 (1966).
8. D. Briggs and M. P. Seah, *Practical surface analysis*, John Wiley & Sons, London (1990).
9. X. Zhang, C. van den Bos, W. G. Sloof, H. Terryn, A. Hovestad, and J. H. W. de Wit, *Surface Engineering*, **20**, 244 (2004).
10. *Operator's multipak software manual - version 6.0*, Physical Electronics Inc., Chanhassen, USA (1998).
11. M. T. Anthony and M. P. Seah, *Surf. Interface Analysis*, **6**, 95 (1984).
12. A. E. Hughes, R. J. Taylor, and B. R. W. Hinton, *Surf. Interface Analysis*, **25**, 223 (1997).
13. J. O. Nilsson, S. E. Hornstrom, E. Hedlund, H. Klang, and K. Uvdal, *Surf. Interface Analysis*, **19**, 379 (1992).



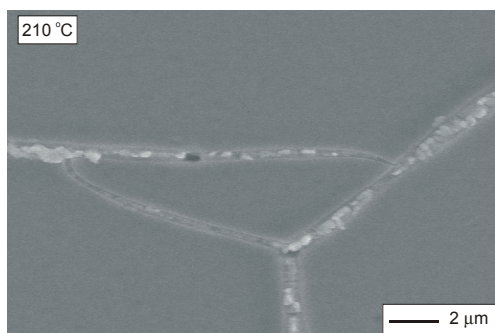
14. B. S. Norgren, M. A. J. Somers, W. G. Sloof, and J. H. W. de Wit, in *12<sup>th</sup> Scandinavian Corrosion Congress & Eurocorr '92*, (P. J. Tunturi, ed.), Vol. 1, p. 139, The Corrosion Society of Finland, Espoo, Finland (1992).
15. X. Zhang, W. G. Sloof, A. Hovestad, E. P. M. van Westing, H. Terryn, and J. H. W. de Wit, *Surf. Coat. Technol.*, **197**, 168 (2005).
16. V. Barranco, S. Feliu, and S. Feliu, *Corros. Sci.*, **46**, 2203 (2004).
17. L. M. Baugh, *Electrochimica Acta*, **24**, 657 (1979).
18. M. Kendig and S. Jeanjaquet, *J. Electrochem. Soc.*, **149**, B47 (2002).
19. M. P. Gigandet, J. Faucheu, and M. Tachez, *Surf. Coat. Technol.*, **89**, 285 (1997).
20. L. Xia, E. Akiyama, G. Frankel, and R. McCreery, *J. Electrochem. Soc.*, **147**, 2556 (2000).



(a) EGCr60

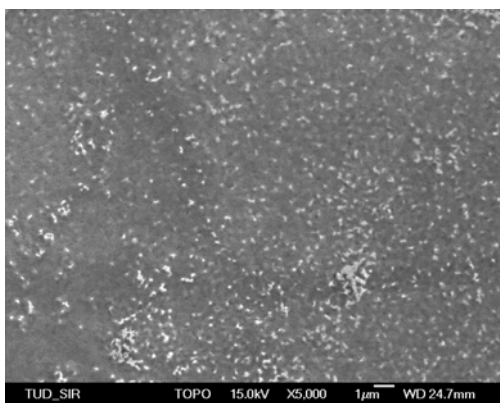


(b) EGCr110



(c) EGCr210

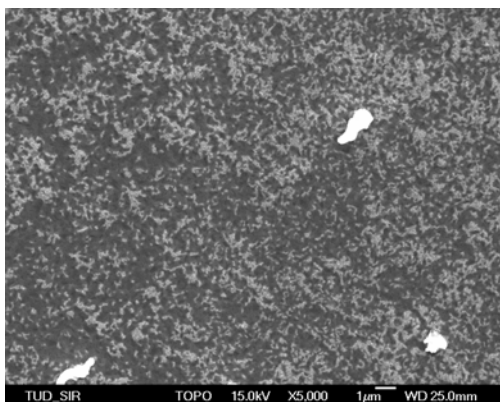
Fig. 1 SEM images for Cr(VI) treated EG steel (10 sec.) heated in an oven at different temperatures: (a) 60°C, (b) 110°C and (c) 210°C, for 30 minutes.



(a) EGCr3-70



(b) EGCr3-110



(c) EGCr3-210

Fig. 2 SEM images for Cr(III) treated EG steel (60 sec.) heated in an oven at (a) 70, (b) 100 and (c) 210°C for 30 min.

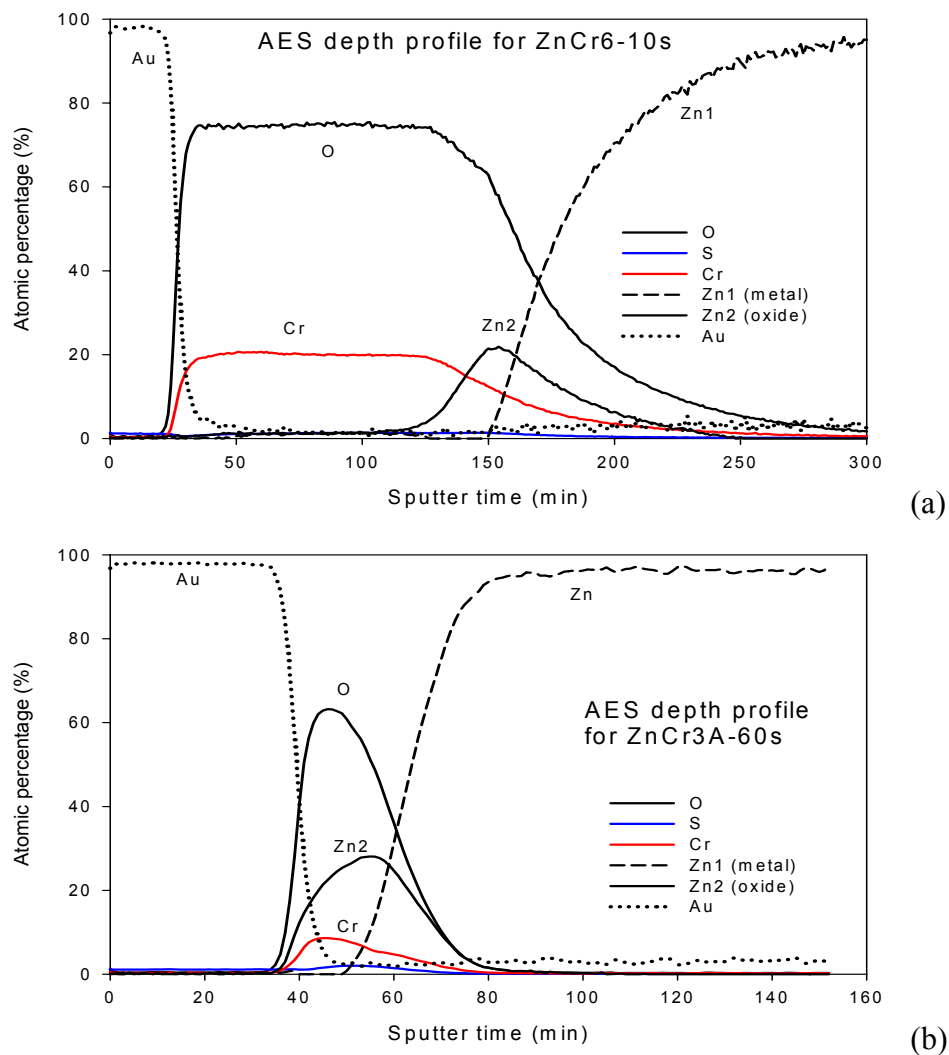


Fig. 3 AES depth profile analyses for (a) Cr(VI) and (b) Cr(III) treated zinc.

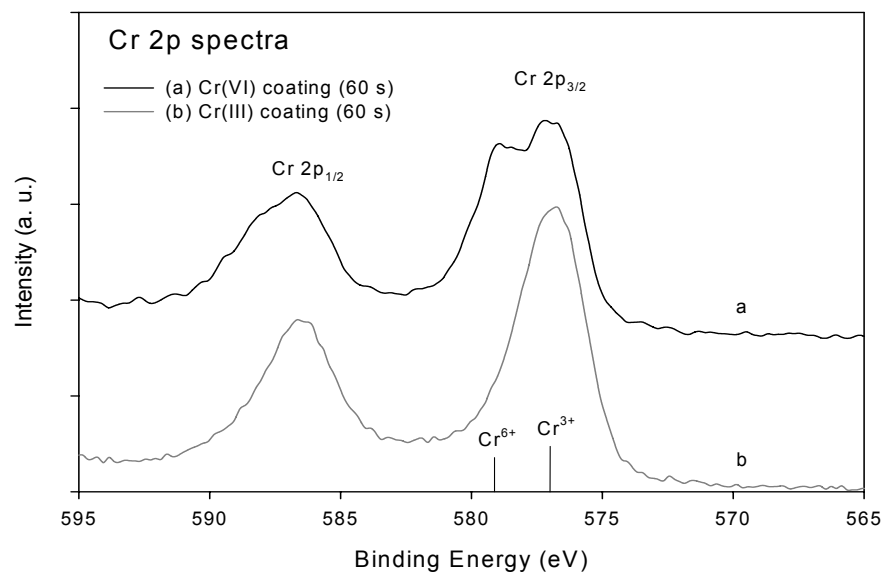


Fig. 4 Cr 2p XPS spectra for Cr(VI) and Cr(III) treated zinc.

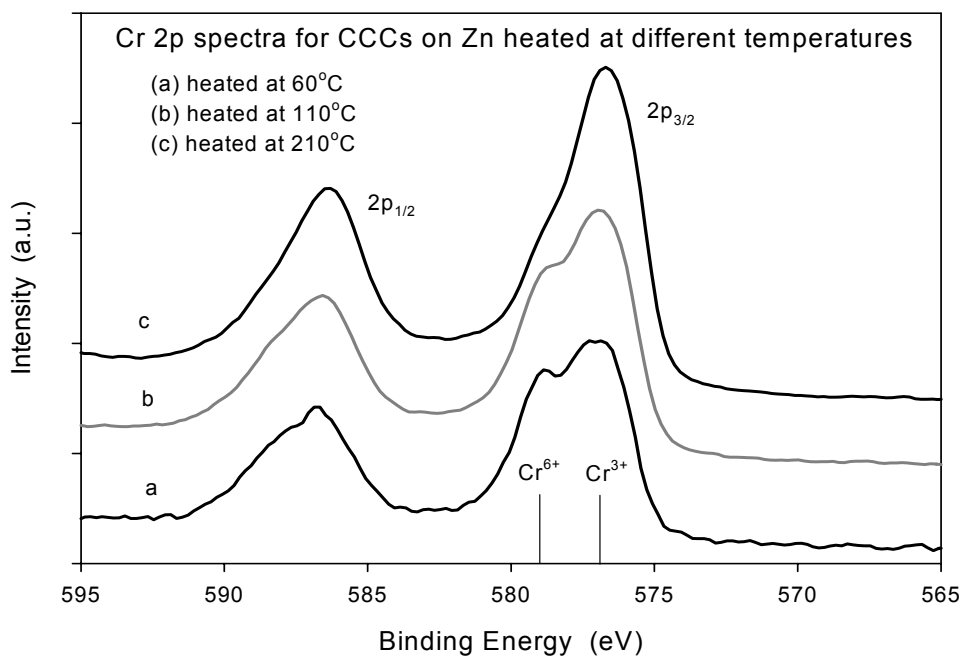


Fig. 5 Cr2p XPS spectra for Cr(VI) treated Zn (10 sec.) heated at different temperatures.

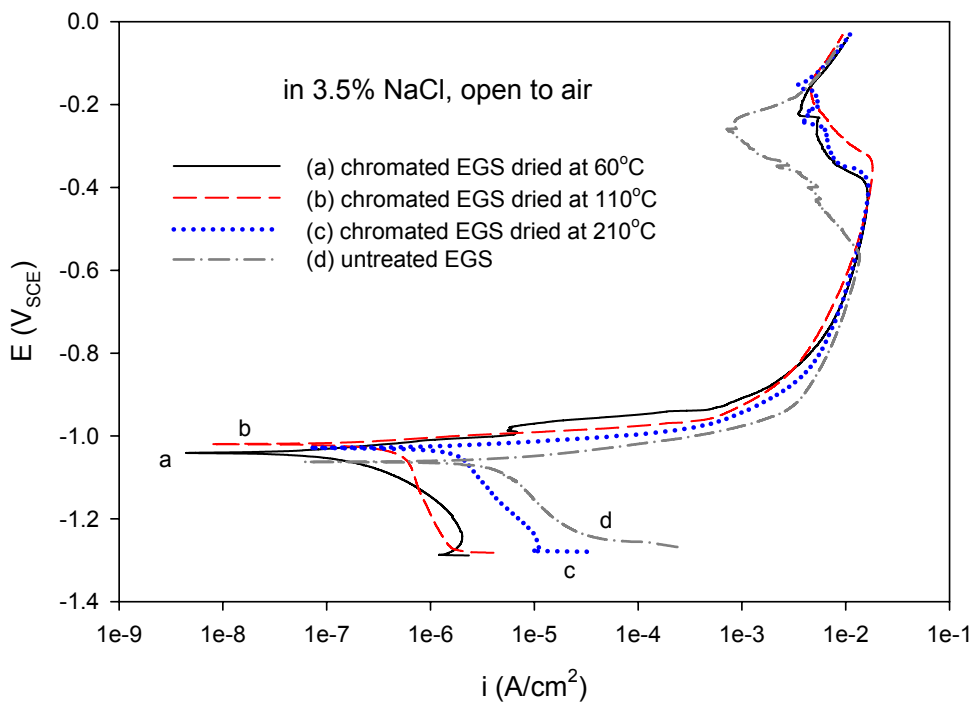


Fig. 6 Polarization curves for Cr(VI) treated EGS (10 sec.) heated at different temperatures and untreated EGS.

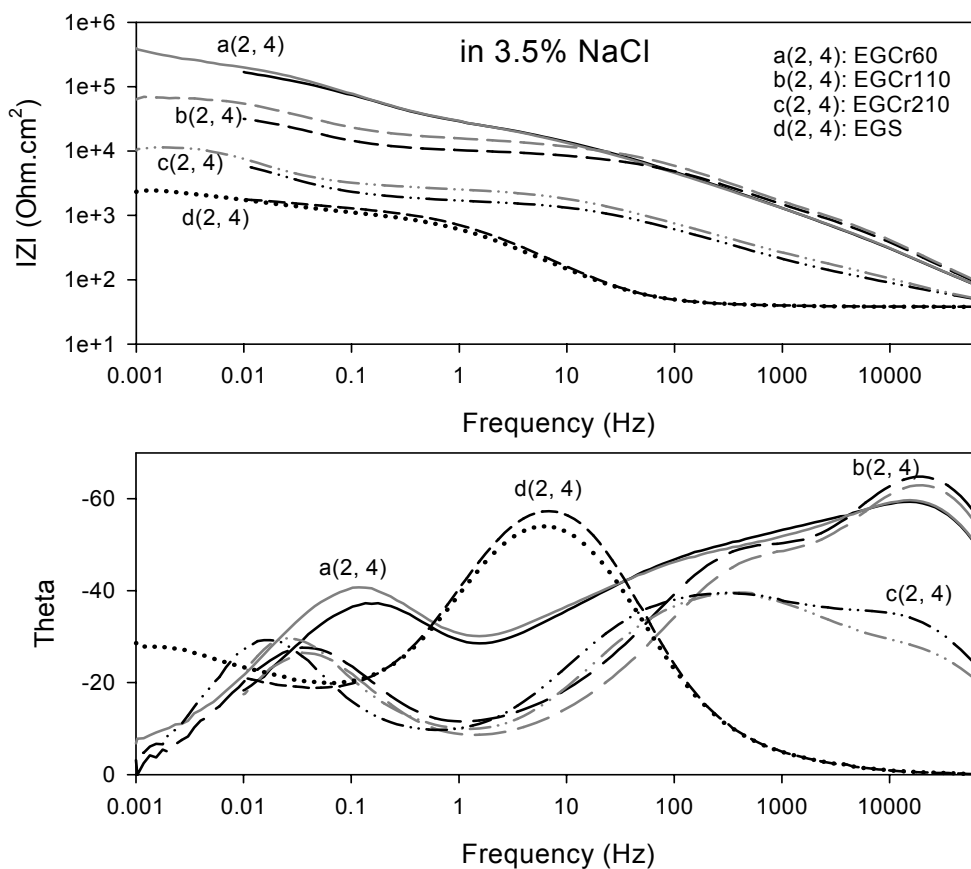


Fig. 7 Bode impedance plots for the Cr(VI) treated EGS specimens (10 sec.) heated at different temperatures, obtained after immersion in the solution for 2 and 4 hrs.

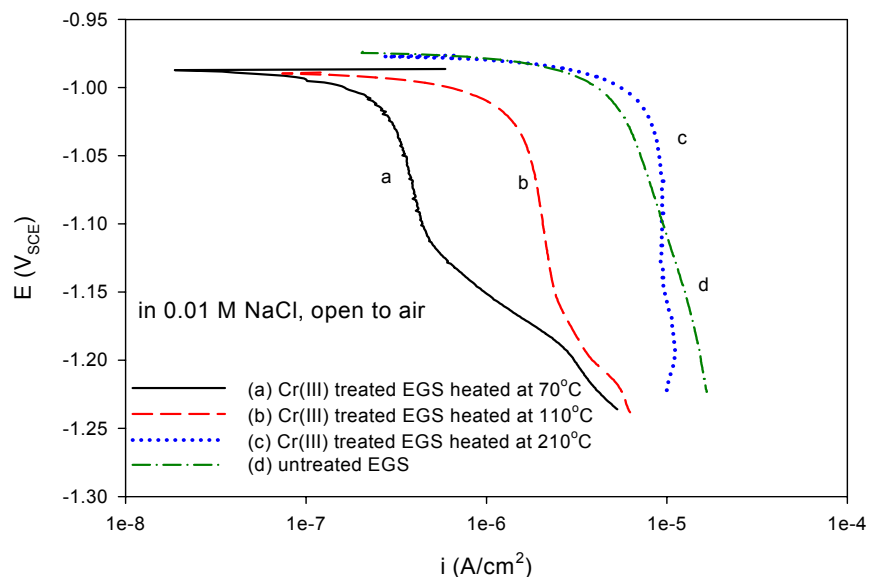


Fig. 8 Cathodic polarization curves measured in 0.01 M NaCl solution (pH 6) for Cr(III) treated EGS heated at different temperatures and for untreated EGS.